AO26: Testing the potential for space-based monitoring of air pollution

Candidate number: 463757
Supervisors: Dr. J. Walker, Dr. A. Dudhia
Word count: 5348

Abstract

Ammonia is a pollutant gas, emitted predominantly by agriculture and biomass burning. Tracking of the gas in near-real-time is important for government and healthcare research, particularly for air quality and climate change. By using the Infrared Atmospheric Sounding Interferometer (IASI) tracking ammonia is now possible via satellite on a global scale.

The technique developed in this project uses a radiative transfer model to simulate the top of atmosphere radiance measured by IASI. Using this data an optimal estimation of the spectral measurements is derived. These measurements are then used to create a new ammonia detection model, which can be applied to the observed IASI data. This model uses theory which has not previously been applied to the technique of remote sounding, allowing a quantitative analysis to be integrated into its construction.

The data produced can be processed very quickly in near-real-time, with the model used to signal presence of ammonia. The results have been tested on a biomass burning event, the Black Saturday Wildfire in South-East Australia on 7th Feb 2009. This method improves the accuracy of ammonia detection by a factor of $\sim$2.5

1 Introduction

Atmospheric ammonia has more than doubled since 1860 with the rise in agriculture (Krupa, 2003), with 63% now being emitted from this sector; a combination of livestock waste, fertilisers and crops (Galloway et al., 2004). This project aims to look at ammonia release from biomass burning events, large scale one off events releasing high concentrations of the gas. These events alone account for 13% of the global ammonia produced.

Ammonia is very reactive and so has a short atmospheric lifetime. This results in a large proportion undergoing dry deposition and being removed from the atmosphere. However, a significant amount also forms particulate ammonium, which has very damaging effects on health and the environment. Particles in the atmosphere are categorised by their size, and particles less than $10_{\mu m}$ (known as particulate matter, PM_{10}) in diameter are considered dangerous since they are small enough to pass through the nose and into the lungs (Environmental Protection Agency, 2012). Ammonium nitrates and sulphates fit into the smaller, fine particulate category, less than $2.5_{\mu m}$ in diameter. This form is even more dangerous as it enters the body and lungs more easily. It has been linked to many respiratory and lung-based problems, such as aggravated asthma, bronchitis, irregular heartbeat, and other breathing difficulties, and is most severe to those with heart and lung disease (Environmental Protection Agency, 2012). In parts of America ammonium sulphate has been recorded to make up as much as 60% of $PM_{2.5}$ in the atmosphere. This particulate matter is long-lived ans so is capable of travelling long distances, having a large effect on acidification of both oceans and soil (Krupa, 2003). Acidification is the effect of the pH lowering of oceans or soil, by an increase in the abundance of H^+ ions present. The

release of ammonia is controlled by the United Nations Economic Commision for Europe's (UNECE) Convention on Long-range Transboundary Air Pollution (UNECE, 1999), though it is not currently enforceable with current ability to detect ammonia.

Currently, it is possible to obtain full retrievals of atmospheric quantities of ammonia from satellite data, but these methods are slow due to the high intensity of radiative transfer calculations required. For fast and up to date information, near-real-time techniques are required, such as (Moore & Holden, 2012). However, progress still needs to be made; Monitoring Atmospheric Compositon and Climate (MACC), a department providing atmospheric information to policy makers and public authorities, does not yet include ammonia in its data (Global Monitoring for Environment and Security, 2012). This lack of information is due to the fact that near-real-time methods using satellite based measurements have only recently been achieved.

IASI scans each region of Earth twice a day, detecting the top of atmosphere radiance, which can be converted to brightness temperature using the Planck function. A simple approach to analyse the satellite data for the detection of ammonia is the brightness temperature Difference (BTD) approach. Absorption of Earth's radiation in the atmosphere is dominated by water vapour and certain major gases such as CO_2, O_3 and CO; their absorption peaks are roughly 100 times larger than those of ammonia.

In simple terms the BTD approach involves selecting two wavenumber channels, one where the ammonia profile shows an absorption peak, and the other where there is minimal ammonia absorption. The idea of a BTD approach is best explained by hypothesising the 2 perfect channels. Take the 2 channels, with a big difference in ammonia in detection. In a perfect scenario, the absorption due to all other gases would be identical in both of these channels. In this case, when we take substract one from the other, the difference will be entirely due to ammonia absorption. The magnitude of the difference then provides a scale for the magnitude of ammonia detected. This is called a 2 channel method, but it also possible to extend this technique to 3 or 4 channels. This process of choosing the channels by eye is a qualitative technique, but this project aims for the first time to choose the channels quantitatively, by developing an algorithm to pick the two optimal channels.

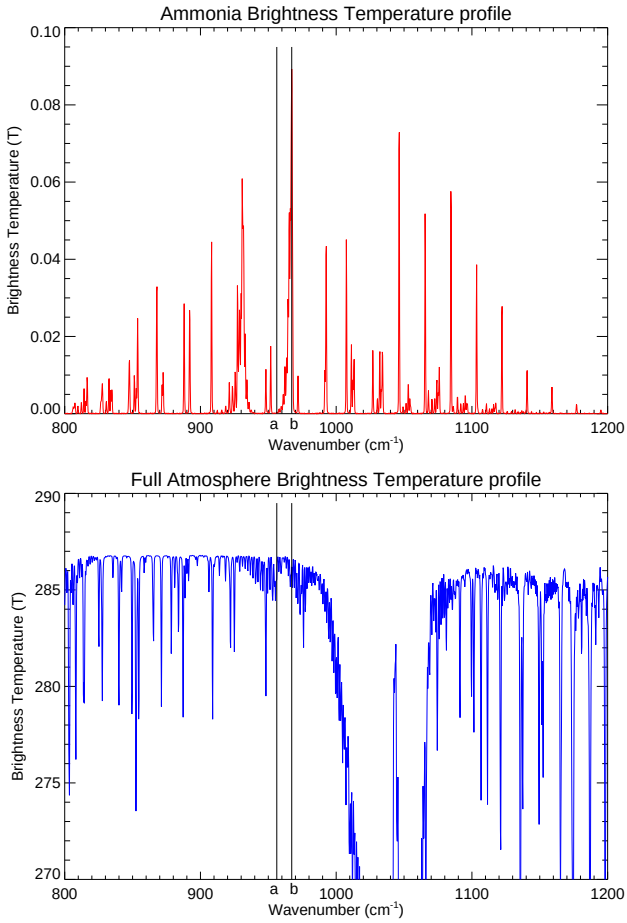

Figure 1: *The brightness temperature profiles for: Red - Ammonia; Blue - The whole atmosphere. Channel B is selected as a peak in ammonia absoprtion, whereas Channel A is at a minimum. They also have a similar brightness temperature through the whole atmosphere, making them a good pair of channels for the Britghtness Temperature Difference technique.*

The aim of this project is to improve the current accuracy of the best existing BTD method for ammonia detection, a three channel technique used by Clarisse (Clarisse et al., 2009). However, as these existing methods are qualitative, their channel contributions are balanced empirically without a mathematical framework. This

project aims to use quantitative methods in the channel selection. I will start by selecting 2 channels by eye, then perform an error analysis to pick out the best possible two channel combination. Once suitable, I will adapt this to a three channel technique, and compare my results to those of the existing methods.

1.1 IASI

The Infrared Atmospheric Sounding Interferometer on board the MetOp-A satellite was launched on October 19, 2006. It measures the spectral radiance emitted by Earth, which is then downloaded for analysis on the ground. Using the Planck Function it can be converted to Brightess Temperature, from which we can obtain information on the atmospheric composition. The satellite orbits the Earth approximately 14 times per day at 800km above its surface. With a swath width of 2200km, it has full global coverage twice per day (Clerbaux et al., 2009).

In the instrument, a Michelson Interferometer decomposes the incoming beam into a broad spectrum, which are sorted into three spectral bands by a cold box. These bands then pass through a Digital Processing Subsystem, which takes the inverse Fourier transform. The output spectra are then transmitted to Earth. It covers a spectral range of 645-2760cm^{-1}, with an apodised spectral resolution of 0.5cm^{-1} and a spectral sampling grid of 0.25cm^{-1}. I shall look at the region of the majority of ammonia absorption (Clarisse et al., 2009), 800-1200cm^{-1}, spanning a total of 1600 IASI channels.

1.2 Radiative Transfer

Using a forward model (Dudhia, 2008), we can calculate the brightness temperature observed at the top of the atmosphere by specifying atmospheric and surface conditions. We can also perform the reverse process to obtain gas retrievals, by comparing measured and modelled spectra.

Consider monochromatic light (light of a narrow range of wavenumbers, ν to $\nu + \delta\nu$) passing though a slab of atmosphere of thickness dz. A

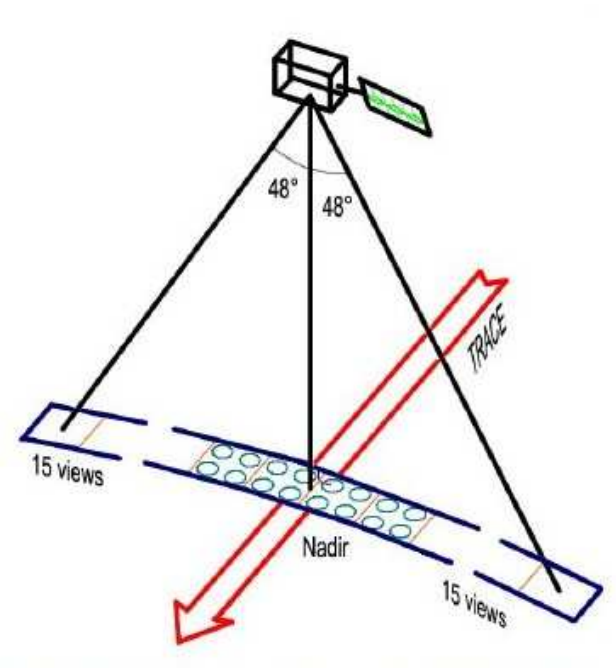

Figure 2: *Diagram showing how the IASI instrument scans the Earth. As it travels along the trace 800km above the Earth it scans side to side with a swath width of 2200km, measuring the observed spectral radiance. Image courtesy of: (Clerbaux et al., 2009)*

certain fraction of light will be absorbed, dependent on the absorber density of the gas, $\rho_a(z)$, the extinction coefficient, $k_\nu(z)$, and also the intensity of incoming light itself, the spectral radiance, L_ν. The extinction coefficient is something that needs to be considered very carefully, what causes a gas to absorb or more or less light at a certain wavenumber? The monochromatic extinction coefficient is in fact dependent on every gas present in the atmosphere, the abundance of each gas at that altitude, and their absorption profile. We will consider the importance of this later. Firstly, the change in monochromatic light dL_ν over atmospheric thickness dz is:

$$\frac{dL_\nu}{dz} = -k_\nu(z)\rho_a(z)L_\nu(z), \qquad (1)$$

which is known as Lambert's Law.

The slab will also emit radiation, dependent on its source function, $J_\nu(z)$, as:

$$\frac{dL_\nu}{dz} = +k_\nu(z)\rho_a(z)J_\nu(z), \qquad (2)$$

where we assume no scattering and that thermodynamical equilibrium applies, and the atmosphere emits as a blackbody, such that $J_\nu(z) = B_\nu(T)$. This has the importance consequence that the radiation emitted by the atmosphere is proportional to temperature.

Combining these equations we obtain Swarzschild's equation for the net change in radiance across the slab of atmosphere,

$$\frac{dL_\nu}{dz} = -k_\nu(z)\rho_a(z)\Big(L_\nu(z)dz - B_\nu(T)\Big) \quad (3)$$

Integrating over all slabs from the surface of the Earth to the top of the atmosphere, gives the spectral radiance detected by the satellite,

$$L_\nu = \int_0^\infty B_\nu(T(z))\frac{\partial\tau_\nu(z,\infty)}{\partial z}dz + B_\nu(T_g)\tau_\nu(0,\infty), \quad (4)$$

where T_g is the ground temperature, and $\tau(a,b)$ is the transmittance between height a and b. The transmittance is the fraction of radiation emitted at a that reaches b, calculated by

$$\tau(a,b) = exp\Big(-\int_a^b k_\nu(z)\rho_a(z)dz\Big). \quad (5)$$

Therefore, by consideration of radiative transfer and with information on absorption spectra and atmospheric composition we can calculate the spectral radiance we expect to see at the top of the atmosphere. A Forward Model has has been developed at the University of Oxford (Dudhia, 2008) based on the absorption spectra as calculated in the HIgh-resolution TRANsmission molecular absorption database (HITRAN).

Although very accurate, the line by line model takes a long time to run, well beyond the scope of real time. This is due to the computationally intense method of calculating the absorption coefficient, $k_\nu(z)$. At wavenumber, ν, the absorption coefficient is a sum of contributions from all spectral lines, as the tails of the Gaussian distributions cannot be neglected,

$$k(\nu)_j = \Sigma_i S_{ij} g(\nu - \nu_i)_j. \quad (6)$$

The transmittance must then be summed over the whole spectral range, where the amount of aborber, u_j, in the atmospheric path, j, needs to be considered. Finally we need to consider all the other absorbers in the atmosphere, and by Beers Law the total transmittance is taken to be a product of the transmittance of each absorber. These calculations are not possible in near real time, hence faster methods are required for research.

Given any atmospheric conditions, such as gas vertical profiles, surface and atmospheric temperatures and layers of cloud for example, the line by line model goes runs all calculations and after a couple of hours produces a brightness temperature plot. The Reference Forward Model (Dudhia, 2008) is used extensively throughout this project, to calculate brightness temperatures for various atmospheric scenarios. It is based on simulations from this model that the optimal channels are selected for ammonia detection.

1.3 Ammonia retrieval

The forward model, $\mathbf{F}$, calculates a predicted value of the spectral radiance, $\mathbf{F}(x, \mathbf{b})$, based on an estimate of the true value of the state, or truth, x, and a best estimate of other factors affecting the measurement, $\mathbf{b}$, such as temperature, atmospheric composition and cloud layers. In this case the state, x, is the quantity of atmospheric ammonia.

The measured value of the spectral radiance, y, as observed by IASI, is given by

$$\mathbf{y} = \mathbf{k}x + \boldsymbol{\epsilon}_{rnd} + \boldsymbol{\epsilon}_{sys}, \quad (7)$$

where $\mathbf{k}$ is the Jacobian, describing how the spectral radiance changes with changes in the state, $k_{ij} = \frac{\partial y_i}{\partial x_j}$; $\boldsymbol{\epsilon}_{rnd}$ is the systematic error due to instrument noise; and $\boldsymbol{\epsilon}_{sys}$ is the error due to uncertainties in $\mathbf{b}$, which can be estimated by climatological variability.

The measurement error covariance, $\mathbf{S}_\epsilon$, given by

$$\mathbf{S}_\epsilon = E\{\boldsymbol{\epsilon}_{rnd}\boldsymbol{\epsilon}_{rnd}^T + \boldsymbol{\epsilon}_{sys}\boldsymbol{\epsilon}_{sys}^T\}, \quad (8)$$

where E is the expected value operator. The diagonal elements are the variance, with the off-diagonal elements giving the covariance, thus

providing information on how the spectral elements are correlated. The matrix as a whole contains information on how the errors weight the spectral measurements.

We now make the assumption that errors are entirely random, such that the probability density function for the spectral radiance, $\mathbf{y}$, is a Gaussian. Although we have just stated $\boldsymbol{\epsilon}_{sys}$ is a systematic error, we can assume it to have a well defined mean and standard deviation, the necessary qualities for a Gaussian distribution.

The probability distribution function (pdf) of obtaining $\mathbf{y}$ given x, $P(\mathbf{y}|x)$ (Rodgers, 2000), goes as

$$P(\mathbf{y}|x) \propto \exp\Big(\frac{1}{2}(\mathbf{y}-\mathbf{F}(x))^T\mathbf{S}_\epsilon^{-1}(\mathbf{y}-\mathbf{F}(x))\Big), \tag{9}$$

where in notation the $\mathbf{b}$ term has been dropped from $\mathbf{F}(x,b)$.

The maximum likelihood estimate of the state, $\hat{x}$, is the value of x at which the pdf is maximised, ie where the exponent is minimised.

In order to minimise the exponent we make the assumption that the forward model is linear. This allows us to express

$$\mathbf{F}(x) \simeq \mathbf{k}x. \tag{10}$$

Using this expression, we can now minimise the exponent of the pdf to find $\hat{x}$,

$$\hat{x} = (\mathbf{k}^T\mathbf{S}_\epsilon^{-1}\mathbf{k})^{-1}\mathbf{k}^T\mathbf{S}_\epsilon^{-1}\mathbf{y}, \tag{11}$$

known as the optimal least squares solution.

Now, subbing in equation 7 and defining $\boldsymbol{\epsilon} = \boldsymbol{\epsilon}_{rnd} + \boldsymbol{\epsilon}_{sys}$, we obtain

$$\hat{x} = (\mathbf{k}^T\mathbf{S}_\epsilon^{-1}\mathbf{k})^{-1}\mathbf{k}^T\mathbf{S}_\epsilon^{-1}(\mathbf{k}x+\boldsymbol{\epsilon}), \tag{12}$$

$$\hat{x} - x = (\mathbf{k}^T\mathbf{S}_\epsilon^{-1}\mathbf{k})^{-1}\mathbf{k}^T\mathbf{S}_\epsilon^{-1}\boldsymbol{\epsilon}, \tag{13}$$

allowing us to define the retrieval gain matrix, $G \equiv (\mathbf{k}^T\mathbf{S}_\epsilon^{-1}\mathbf{k})^{-1}\mathbf{k}^T\mathbf{S}_\epsilon^{-1}$, such that $\hat{x} - x = \mathbf{G}\boldsymbol{\epsilon}$.

This important result is the basis for our quantitative method in developing the ammonia flag. The difference between the maximum likelyhood state, $\hat{x}$, and the true state, x, is given by $\mathbf{G}\boldsymbol{\epsilon}$.

We can now evaluate the retrieval error variance,

$$\sigma_{\hat{x}}^2 = E\Big\{\{\hat{x}-x\}\{\hat{x}-x\}^T\Big\} = \mathbf{G}\boldsymbol{\epsilon}\boldsymbol{\epsilon}^T\mathbf{G}^T = \mathbf{G}\mathbf{S}_\epsilon\mathbf{G}^T \tag{14}$$

It is this retrieval error that we shall seek to minimise in order to detect the presence of ammonia.

Importantly, assuming all the errors are uncorrelated, the retrieval error can be decomposed into separate errors

$$\sigma_{\hat{x}}^2 = \Sigma_i\sigma_{\hat{x}_i}^2 = \mathbf{G}(\Sigma_i\boldsymbol{\epsilon}_i\boldsymbol{\epsilon}_i^T)\mathbf{G}^T \tag{15}$$

This allows us to see which error is most prominent, which is useful when breaking down the analysis. For example if CO_2 absorption is very high in a certain wavenumber channel, a 1σ perturbation representing the unknown exact quantity of CO_2 in the atmosphere may cause the largest error in the retrieval. Similarly it could be the unknown atmospheric temperature, or the instrument error.

The next step is to develop an algorithm to find the two wavenumber channels for which the retrieval error variance is minimised.

1.4 Existing Ammonia detection algorithms

The brightness temperature Difference (BTD) technique is the most effective fast method for analysing IASI data in detection of trace gases. It has been used for detecting SO_2 (Walker et al., 2012), which in volcanic eruptions can be used to track volcanic ash, a serious aviation hazard. This has been developed to a four channel technique, used by the European alert (Rix et al., 2009).

In NH_3 detection Clarisse has developed a 3 channel technique using a sensitive ammonia channel at 867.75cm^{-1} and two insensitive ammonia channels at 861.25cm^{-1} and 867.75cm^{-1} (Clarisse et al., 2009). However, these channels are chosen by eye, without any quantitative method of selection, and are therefore unlikely to be the best channels possible. Another technique has been developed with inclusion of various parameters in the determination of $\mathbf{S}_\epsilon$ (Walker et al., 2011). These parameters include column perturbations to atmospheric components such as water vapour, ozone, carbon dioxide as well as the atmospheric temperature. They also include a 20K surface temperature perturbation and cloudiness modelled as 15 optically

thick layers at 1km intervals. However, although this analysis is performed, it is still not used to select channels for a brightness temperature Difference technique.

The new method aims to combine the two, developing an algorithm using parameters discussed (Walker et al., 2011), to select three channels (Clarisse et al., 2009), now via a quantitative method.

2 Developing an Ammonia detection algorithm

To use a brightness temperature Difference technique, such as in Fig. 1, I needed brightness temperature profiles of the whole atmosphere, and of each individual gas. Every time the atmospheric conditions were changed, I had to adapt the forward model to produce data for the top of atmosphere radiance, and convert this to brightness temperature.

Firstly, I modelled the atmosphere based on an atmosphere containing the six major gas absorbers: CO_2, H_2O, O_3, CO, CH_4 and N_2O; with standard daytime vertical profiles for each gas (Remedios et al., 2007). At standard climatological conditions other gases have negligible effect on the overall brightness temperature (Coheur et al., 2009). This provides the profile we see in Fig. 3. To see the effect of each individual gas, the RFM was run with each gas removed one at a time. From Fig. 3, we can see that an atmosphere without H_2O has a much smoother profile than the whole atmosphere, and the removal of ozone takes out the large feature from 1000-1100cm^{-1}, known as the ozone band. Taking the difference between the full atmosphere profile and the profile with one gas removed allowed me to single out the aborption profile of each gas, and produce the plots in Fig. 4. We can see the ammonia has a very spiky profile, and most notably the peaks are ∼200 times smaller than those of water vapour. It is this difference in scale that makes detection of ammonia via this method so difficult, as we need channels where the difference in the size of ammonia peaks is much greater than the difference in water vapour or other gases.

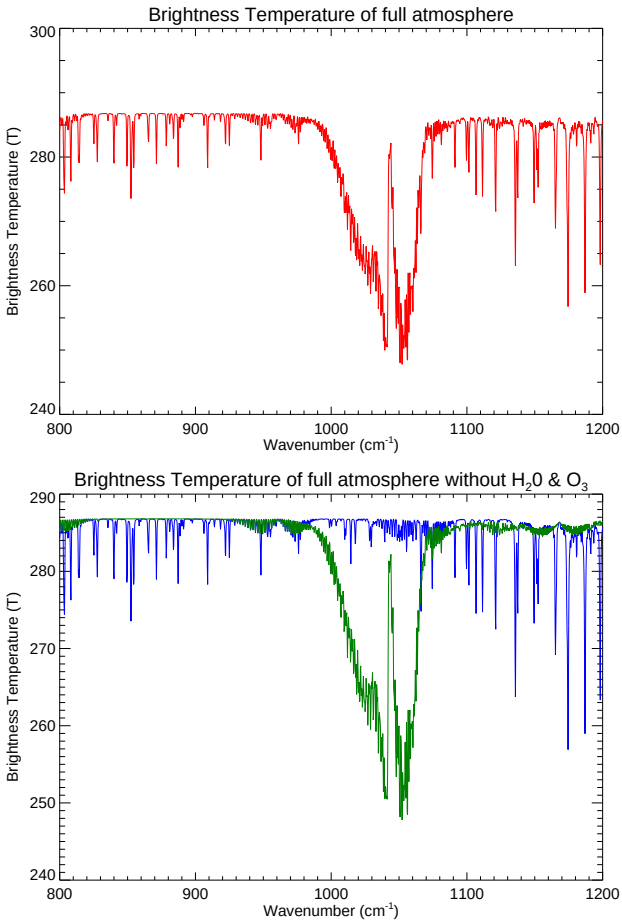

Figure 3: *The brightness temperature profiles for: Red - a full atmosphere (which I will define as BT_{all}) containing CO_2, H_2O, O_3, CO, CH_4 and N_2O; Blue - without H_2O (defined as BT_{H_2O}); and Green - without O_3 (BT_{O_3})*

The plots in Fig. 4 are sufficient to select channels by eye, as will be used in Method 1, but fail to make use of the retrieval error variance, $\sigma_{\hat{x}}^2$ (equation 14), in the selection method. Methods 2 and 3 will then develop this into an automated channel selection technique, minimising the retrieval error of all possible combinations of channels for 2 and 3 channels respectively.

2.1 Method 1 - 2 channel selection by eye

I began with a 2 channel technique, choosing the channels by eye. The aim being to maximise

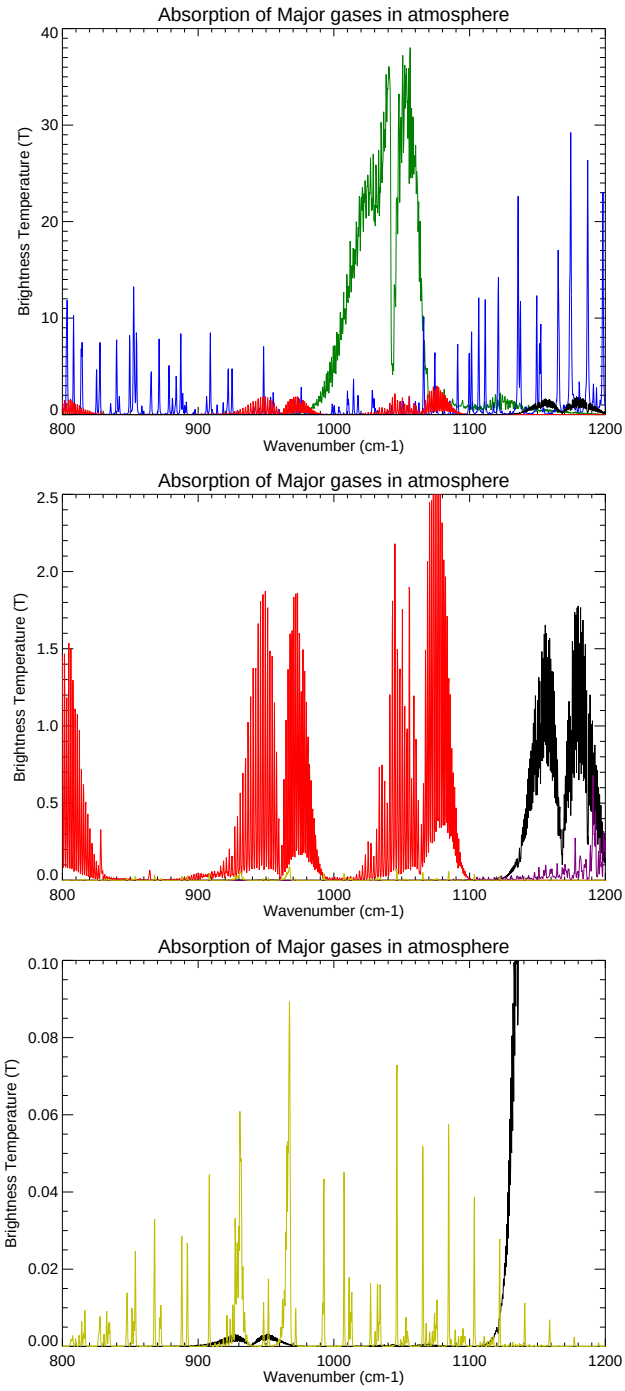

Figure 4: *Brightness temperature contributions from each individual gas, calculated by BT_{all} - BT_{gas}: Green - O_3; Blue - H_2O; Red - CO_2; Black - N_2O; Purple - CH_4 and Yellow - NH_3.*

the difference in ammonia temperature, but minimise the difference in all other gases. I started by choosing the ammonia peaks above 0.02K from Fig. 4 as channel A, and a nearby minimum as B, and calculating the retrieval error variance, $\sigma^2_{\hat{x}}$, for each pair of channels. I then looked closer at each pair of channels, and altered any channels overlapping with absoption peaks from other gases. Above 1000cm^{-1}, I found that the ozone band and water vapour profiles interfered too heavily. The best pair of channels I found to minimise the error, $\sigma^2_{\hat{x}}$, were at 967.25cm^{-1} and 969.75cm^{-1}.

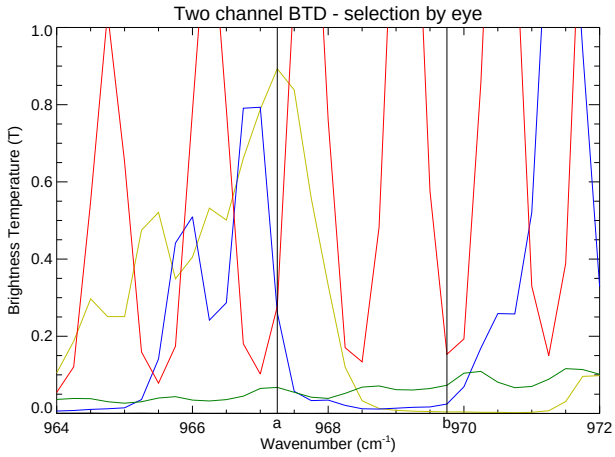

Figure 5: *Fig. 4 zoomed in to a spectral window 964 - 972cm^{-1}. The BT profiles are the same: Green - O_3; Blue - H_2O; Red - CO_2; and Yellow - NH_3. However, the yellow NH_3 has been enhanced by a scale factor of 10. Channel A is an ammonia peak 967.25cm^{-1}, and Channel B is a minimum at 969.75cm^{-1}*

Fig. 5 shows these two channels in detail, with the ammonia peaks enhanced by a factor of 10 to make them clearer. Although there are CO_2 lines, and a large H_2O peak in the spectral region, the two channels have a very similar CO_2 temperature, and since channel A is at the largest ammonia peak, the error was minimised.

2.2 Method 2 - automated 2 channel selection

Selecting the channels by eye was a useful development tool, but it is not extensive. Out of $1600^2/2$ possible pairs of channels I considered approximately 30. Moreover, for each peak I only considered a pair channel close to the peak, rather than search the whole spectrum for a bet-

ter match. Therefore, I developed a programme to scan all possible pairs of channels, in order to minimise the error.

Since the criterion for choosing the best 2 channels is to minimise the retrieval error covariance, I then developed a programme to select the optimal pair based on this criterion. Firstly, this required careful thought of the errors to be considered. There are numerous variables which are unknown beyond a certain degree of accuracy. These parameters include vertical profiles for each atmospheric gas, surface and atmospheric temperature, cloud layers and instrument error from IASI. They all had to be included in the measurement error covariance, $\mathbf{S}_\epsilon$.

For each variable being considered, I had to take into account an upper margin for error, for example 1σ above the climatological value, and calculate the brightness temperature profile for the perturbed quantity. With all other parameters held constant, I could then calculate the brightness temperature profile including the error, by running the input parameters through the forward model. Again, I took the difference between the new profile and the standard atmospheric profile in Fig. 3, to find the profile for just the individual error in question (as for each gas in Fig. 4).

Going back to equation 8, all of the errors mentioned are systematic errors, other than the one random error due to the IASI instrument; we can therefore reexpress the equation as:

$$\mathbf{S}_\epsilon = E\{\boldsymbol{\epsilon}_{rnd}\boldsymbol{\epsilon}_{rnd}^T + \Sigma_i(\boldsymbol{\epsilon}_{sys_i}\boldsymbol{\epsilon}_{sys_i}^T)\}. \qquad (16)$$

The follwing parameters are included in the automated channel selection:

1. Gas vertical profiles. In order to incorporate the unknown quantity of each gas in the atmosphere, I took a 1σ perturbation as a reasonable approximation to the error. This alters the quantity of gas by 1σ all the way through the vertical column, which assumes that the gas is vertically correlated over the entire depth of atmosphere. Although this does not hold in general, it is a good first order approximation.

2. Atmospheric temperature. For atmospheric temperature I used the same technique as for the gases, based on a 1σ perturbation. The importance of atmospheric temperature comes from equation 2, where the source function emits as a blackbody. The intensity of emission is dependent on temperature, hence the importance of the temperature throughout the atmosphere.

3. Surface temperature. The surface temperature is slightly different to model, the forward model contains a surface temperature flag (Dudhia, 2008), which I increased by 10K. The magnitude by which to vary these parameters is approximate, but they all should be altered by a similar proportion. A 10K perturbation is roughly 1σ in magnitude, and approximately equates the diurnal variation over a daily cycle in this region.

4. Random error. This is the defined instrument error which is a known quantity for the IASI instrument.

5. Cloud layers. The meteoroligcal conditions are unknown, and as such require the largest approximations. Cloud layers in remote sounding obscure the features of the surface and atmosphere below. I modelled the cloud layers to be situated at 1km intervals from 1km-12km in the atmosphere. They are all assumed to be independent, and are modelled as three different types of layer: optically thick, optically thin and partial cloud (a mixture of optically thick cloud and no cloud).

Finally, I also computed the jacobian for ammonia, $\mathbf{k}$, on the forward model. With these errors I could calculate the measurement error covariance, $\mathbf{S}_\epsilon$, and I then had sufficient information to calculate the retrieval error variances using equation 14. After coding a programme to search every pair of channels in my spectral window of 800-1200cm^{-1}, and calculate its retrieval error, $\sigma_{\hat{x}}^2$, I then obtained the optimal pair of channels for ammonia detection via the BTD technique. The selected two channels were 956.25cm^{-1} and 967.5cm^{-1}.

The weighted difference of the 2 channels is a fast method of detecting ammonia from IASI data, the accuracy of which will be discussed in the Results section.

2.3 Method 3 - automated 3 channel selection

The next step was to develop the 2 channel selection method to 3 channels. The theory applied to the automated 2 channel selection technique is unchanged, but the challenge is much more computational. Once the channels have been selected, I need to decide how they are weighted in the detection model. For two channels, a very simple way would be to take the difference. However, for three channels, it is not that simple. To resolve this I took a weighting of the channels using the gain matrix, which I applied to the 2 channel model as well.

Also, with a sampling from or 0.25cm^{-1}, the spectral range of 400 wavenumbers represents 1600 wavenumber channels, so for 3 channels there were $1600^3/3!$ combinations. After a full recoding of the channel selection method from 2 channels to 3, this took approxiamtely 8 hours to run to detect the three optimal channels. The channels chosen were 961.25cm^{-1}, 967.25cm^{-1} and 1074.5cm^{-1}.

3 Results

I am comparing the channels selected by my methods with those of the Clarisse channels (Coheur et al., 2009): 867.75cm^{-1}, 861.25cm^{-1} and 873.5cm^{-1}, as this is the previous method I am aiming to improve on. A weighted difference of each set of channels is used to analyse the IASI data, taken on 7th February 2009, at 9.30am local time. The plots produced from this data are shown in Fig. 7 and Fig. 8.

In all four cases it is immediately obvious there is a large ammonia cloud detected off the south-eastern coast of Australia, due to ammonia emission from the Black Saturday wildfires. However, the key to the accuracy of each method lies not in the region of high ammonia detection, but in regions where we expect little to no atmospheric ammonia. In order to perform the error analysis in the next section, I need a background sample that I can assume to be uniform in emission of ammonia. I have therefore made this assumption for regions outside the wildfire. Although there may be some emissions, they are likely to be small in comparision to the wildfire. This means that the most accurate ammonia flag should minimise the deviation from a uniform background value; any structure outside the wildfire is a sign of an imperfection in the flagging system.

Figure 6: *Satellite view of the Black Saturday Wildfire in visible spectrum, on 7th February 2009 (same day as IASI data being analysed). Photo timed at 11.57, taken from the MODIS Aqua Satellite. (National Aeronautics and Space Administration , NASA)*

At a glance, based on observation of the background detection, it is very difficult to tell the difference between the images. On a large scale the automated 3 channel method looks the best, with the most uniform background colour. The 2 channel automated method is picking up on some fairly regular pattern, particularly in the top left of the image, away from the wildfire. Also, the Clarisse 3 channel method looks to have a slightly more hazy background than the new 3 channel method. However, this is again a qualitative description, and I need to analyse the results quantitatively.

3.1 Error Analysis

To determine which method provides the most reliable flag, an analysis has been performed on the background. There are two errors given in Table 1: the retrieval error, $\sigma_{\hat{x}}$ calculated by the optimal estimation theory, and there is also a signal-noise (S-N) ratio, given by:

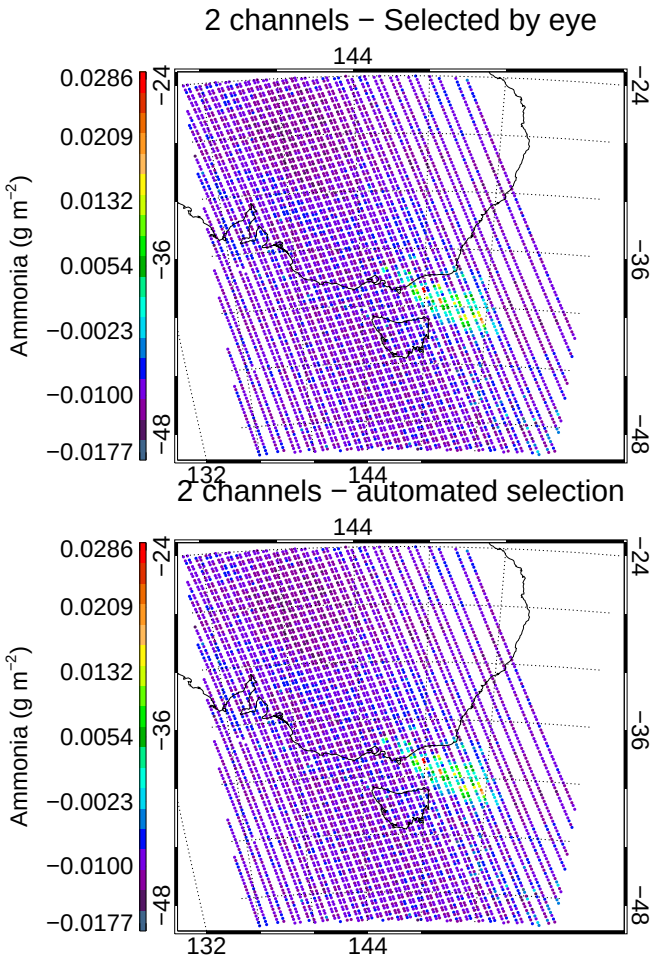

Figure 7: *Black Saturday IASI data - 7th Feb 2009 - New South Wales, Australia. Showing results for detections from: 2 channel by eye method, and 2 channel automation selection method. Note the differences in scale between the two images.*

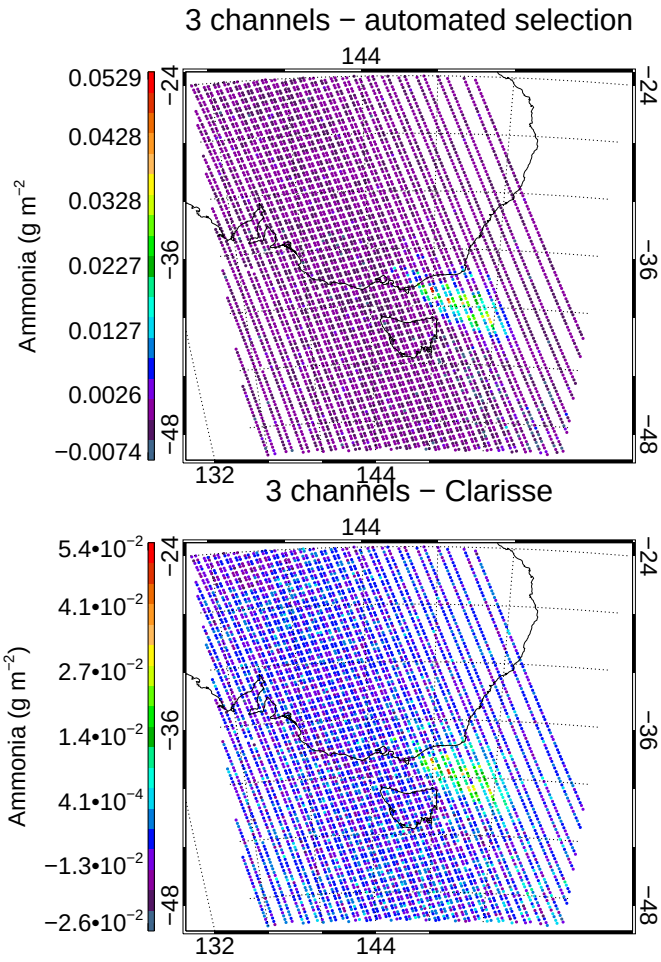

Figure 8: *Black Saturday IASI data - 7th Feb 2009 - New South Wales, Australia. Showing results for detections from: 3 channel automated selection method, and 3 channels as published by Clarisse (Clarisse et al., 2009).*

$$\frac{(\text{Max NH}_3\text{ Peak} - \text{Mean NH}_3\text{ background})}{\text{Standard Deviation NH}_3\text{ background}} \tag{17}$$

The background is defined by the regions where there are no detections of ammonia. To

Method	Retrieval Error, $\sigma_{\hat{x}}$ (mg m^{-2})	Max NH3 Signal (mg m^{-2})	Mean background (mg m^{-2})	Standard deviation (mg m^{-2})	S-N ratio
2 ch - eye	**4.2428**	28.6	-18.22	1.58	**29.69**
2 ch - auto	**1.7662**	47.8	-3.75	1.53	**33.65**
3 ch - auto	**1.5321**	52.9	-0.650	1.26	**42.64**
Clarisse	**3.8432**	54.0	-8.59	3.636	**17.22**

Table 1: *Error Analysis Results for all 4 methods. The Retrieval Error is the error calculated via the optimal estimation theory. The Signal-Noise (S-N) is a ratio of the (peak - mean background) ammonia signal to the standard deviation on the background noise. This is an objective method of measuring the accuracy of the method. The higher the ratio, the more accurate the method is.*

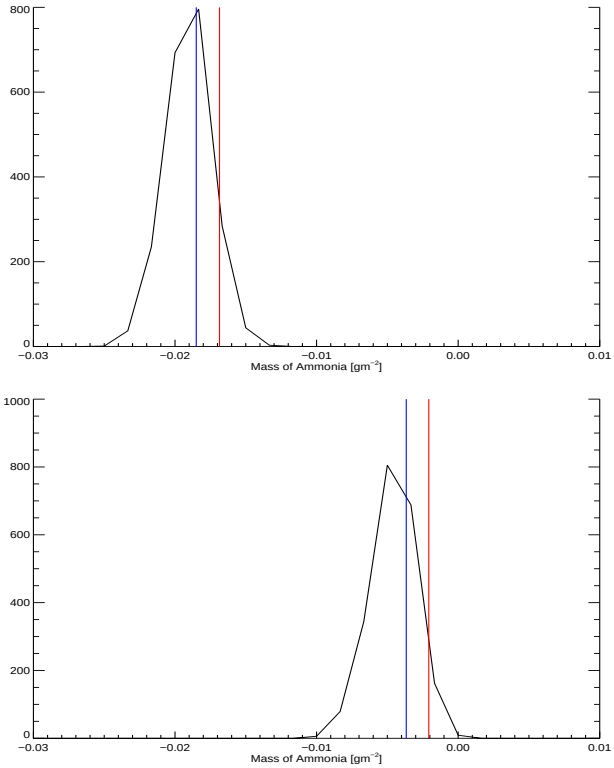

Figure 9: *Histogram plots for the background data, with the y-axis as a measure of frequency per bin, over 25 bins. All points represented are those above 34° latitude from Fig. 7. The plots are for the 2 channel by eye and 2 channel automated methods. In each histogram the blue line is the mean of the background points, and the red line is the mean plus one standard deviation. Both diagrams have a standard deviation ∼1.5 mg m^{-2}, exact values are given in Table 1.*

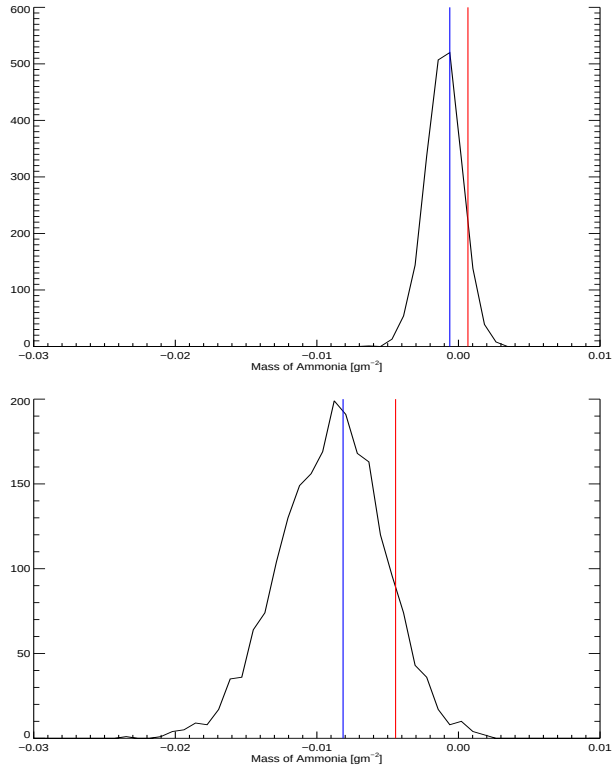

Figure 10: *Histogram plots for the background data. All points represented are those above 34° latitude from Fig. 8.The plots are for 3 channel automated method and the 3 Clarisse channels. In each histogram the blue line is the mean of the background points, and the red line is the mean plus one standard deviation. The new 3 channel method has a standard deviation of 1.26mg m^{-2}, whereas the standard deviation of the Clarisse channels is a much higher 3.64mg m^{-2}.*

select a background sample, one option was to assign a threshold quantity of ammonia to be the definition of a detection, for example 5σ above the mean, and remove all points above this value from the data set. However, defining the cut off point is not possible at a statistically fair level, it will alter the mean and standard deviation of the background sample. Therefore, I have taken the background to be a geographical region, all points above -34° latitude. Although this cuts out more points it does not increase the risk of bias, based on the assumption that the region outside the wildfire should be uniform. Therefore, the best detection method should minimise the variation of these background points. The mean and standard deviations are both calculated based on this set of points above -34° latitude.

The retrieval error in Table 1 shows what we expect; the automated channels have the smallest error since minimising it was the sole criterion for their selection. However, the S-N ratio now provides an objective method, with no bias. Fig.9 and Fig.10 show the spread of points about the background mean for each method. They show that 3 Clarisse channels have the largest standard deviation, while the developed 3 channel method minimises it. From Table 1, we can see that this also leads to the new 3 channel method having the highest signal-noise ratio. The S-N ratio of 42.64 makes it ∼2.5

times more reliable in detecting genuine ammonia points compared with the previous method.

Although the 3 channel method provides the best model for detecting ammonia, it is best used purely as a relative measure. This BTD technique is a very useful method for comparing one point to another, in terms of quantity of ammonia detected. We can use it show one region definitely has a higher quantity of ammonia that another. However, the absolute quantity of ammonia in the atmosphere is still uncertain because of errors in the parameters used. For example, the analysis of the cloud layers is very uncertain. The other issue with this technique is that it is not accurate to localised values. This technique could not pinpoint the factory within a city from which ammonia is being released, but better analyse the regions in a country where agriculture is emitting higher levels of ammonia.

Finally, in determination of an ammonia flag, a threshold level of ammonia must be assigned. Any location with a measured ammonia level beyond this threshold is then classed as a detection. A reasonable threshold is 5σ above the mean of the background. For the automated three channel technique this gives a threshold of 5.65mg g^{-2}. This could be useful for government control, it would be very straight forward to output only results above this threshold.

4 Conclusions

4.1 Summary

The real time detection of ammonia is important for government databases and health organisations for air quality and climate change. Full analysis of the data to break down gases into vertical profiles is time consuming, beyond the scope of real time analysis. This method allows for near real time information on the global tracking of ammonia right from its emission. Although it does not provide accurate information on the absolute value of ammonia emitted, it shows accurately relative levels of the substance. It provides continous data, that can be produced quickly with minimal computing power as the data is received from IASI.

The developed flag has shown improvement on the previous method (Clarisse et al., 2009) by a factor of 2.5, making it the best available method for detecting ammonia using satellite data. Now it has been developed it is also easily transferable to other trace gases, which is important for the same reasons.

4.2 Further Work

There are two obvious ways to continue further work into this research. To improve the ammonia flag the next step would be to move from a 3 channel technique to a 4 channel technique. To choose the 4 channels would require enormous computing power, over a length of days, but once the channels had been chosen the 4 channel method would be just as efficient. Obviously channels can be added in theory until all 1600 are used, but there comes a point where we have reached sufficient accuracy, and 3 or 4 channels is sufficient for most government and health organisations.

Once the flag has been developed sufficiently, we can then use this technique to detect other trace gases in the atmosphere. The technique itself is completely transferrable for all trace gases, in fact the vast majority of error analysis involved is transferrable too. The only work necessary is to run the forward model to obtain the jacobian for any gas being searched for. With this jacobian the channel selection method can easily be run, and once the channels have been chosen IASI data is ready to be analysed in near real time.

Acknowledgement

The author would like to thank Dr. J. Walker, Dr. A. Dudhia for all their valuable expertise and support with this project.

References

L. Clarisse, et al. (2009). 'Global ammonia distribution derived from infrared satellite observations'. *Nature Geosci* .

C. Clerbaux, et al. (2009). 'Monitoring of atmo-

spheric composition using the thermal infrared IASI/MetOp sounder'. *Atmospheric Chemistry and Physics Discussions* **9**.

P.-F. Coheur, et al. (2009). 'IASI measurements of reactive trace species in biomass burning plumes'. *Atmospheric Chemistry and Physics* **9**(15):5655–5667.

A. Dudhia (2008). 'Reference Forward Model (RFM) [Internet]'. `http://www.atm.ox.ac.uk/RFM/`.

Environmental Protection Agency (2012). 'United States Environmental Protection Agency'. `http://www.epa.gov/airquality/particlepollution/index.html`.

J. N. Galloway, et al. (2004). 'Nitrogen Cycles: Past, Present, and Future'. *Biogeochemistry* **70**:153–226. 10.1007/s10533-004-0370-0.

Global Monitoring for Environment and Security (2012). 'Global Monitoring for Environment and Security (GMES)'. `http://www.gmes.info/pages-principales/overview/`.

S. Krupa (2003). 'Effects of atmospheric ammonia (NH3) on terrestrial vegetation: a review'. *Environmental Pollution* **124**(2):179 – 221.

D. Moore & J. Holden (2012). 'Brightness Temperature Difference Detection'. `http://www.leos.le.ac.uk/BORTAS_IASI/BORTAS_index.html`.

National Aeronautics and Space Administration (NASA) (2009). '7 February 2009 MODIS Aqua satellite image of smoke plumes from bushfires burning in Victoria'. `http://rapidfire.sci.gsfc.nasa.gov/subsets/?subset=Australia6.2009038.aqua.250m`.

J. J. Remedios, et al. (2007). 'MIPAS reference atmospheres and comparisons to V4.61/V4.62 MIPAS level 2 geophysical data sets'. *Atmospheric Chemistry and Physics Discussions* .

M. Rix, et al. (2009). 'Satellite Monitoring of Volcanic Sulfur Dioxide Emissions for Early Warning of Volcanic Hazards'. *Selected Topics in Applied Earth Observations and Remote Sensing, IEEE Journal of* **2**(3):196 –206.

C. D. Rodgers (2000). *Inverse Methods for Atmospheric Sounding*. World Scientific Publishing Co.

UNECE (1999). 'The 1999 Gothenburg Protocol to Abate Acidification, Eutrophication and Ground-level Ozone '. `http://www.unece.org/env/lrtap/multi_h1.html`.

J. C. Walker, et al. (2012). 'Improved detection of sulphur dioxide in volcanic plumes using satellite-based hyperspectral infrared measurements: Application to the Eyjafjallajkull 2010 eruption'. *J. Geophys. Res* .

J. C. Walker, et al. (2011). 'An effective method for the detection of trace species demonstrated using the MetOp Infrared Atmospheric Sounding Interferometer'. *Atmospheric Measurement Techniques* .